



# CHORUS

This is the accepted manuscript made available via CHORUS. The article has been published as:

## Unusually large chemical potential shift in a degenerate semiconductor: Angle-resolved photoemission study of SnSe and Na-doped SnSe

M. Maeda, K. Yamamoto, T. Mizokawa, N. L. Saini, M. Arita, H. Namatame, M. Taniguchi, G. Tan, L. D. Zhao, and M. G. Kanatzidis

Phys. Rev. B **97**, 121110 — Published 23 March 2018

DOI: [10.1103/PhysRevB.97.121110](https://doi.org/10.1103/PhysRevB.97.121110)

## **Unusually large chemical potential shift in a degenerate semiconductor: Angle-resolved photoemission study of SnSe and Na-doped SnSe**

M. Maeda,<sup>1</sup> K. Yamamoto,<sup>1</sup> T. Mizokawa,<sup>1</sup> N. L. Saini,<sup>2</sup> M. Arita,<sup>3</sup> H. Namatame,<sup>3</sup>  
M. Taniguchi,<sup>3</sup> G. Tan,<sup>4</sup> L. D. Zhao,<sup>4</sup> and M. G. Kanatzidis<sup>4</sup>

<sup>1</sup>*Department of Applied Physics, Waseda University, Shinjuku, Tokyo 169-8555,  
Japan*

<sup>2</sup>*Department of Physics, University of Roma "La Sapienza", 00185 Roma, Italy*

<sup>3</sup>*Hiroshima Synchrotron Radiation Center, Hiroshima University, Higashi-hiroshima,  
Hiroshima 739-0046, Japan*

<sup>4</sup>*Department of Chemistry, Northwestern University, Evanston, IL 60208, USA*

We have studied the electronic structure of SnSe and Na-doped SnSe by means of angle-resolved photoemission spectroscopy. The valence band top reaches the Fermi level by the Na doping, indicating that Na-doped SnSe can be viewed as a degenerate semiconductor. However, in the Na-doped system, the chemical potential shift with temperature is unexpectedly large and is apparently inconsistent with the degenerate semiconductor picture. The large chemical potential shift and anomalous spectral shape are key ingredients for understanding of the novel metallic state with the large thermoelectric performance in Na-doped SnSe.

The recent discovery of ultrahigh thermoelectric performance in hole-doped SnSe has shown that band engineered SnSe is one of the key materials for the future thermoelectric devices [1]. The IV-VI semiconductors such as PbSe/PbTe [2-6] and SnSe/SnTe [7,8] commonly exhibit high thermoelectric performance with the large Seebeck coefficient due to the multiple valence band maxima and with the suppression of lattice thermal conductivity, which is related to the lattice anharmonicity driven by the unusual hybridization between the Pb(Sn) s, Pb(Sn) p, and chalcogen p orbitals [2]. The Seebeck effect of SnSe is enhanced by the smaller energy separation between the multiple valence band maxima [8]. SnSe has a layered structure constructed with strong bonds along the b-c plane and weak bonds along the a-axis as shown in Fig. 1(a). SnSe has a reversible structural phase transition around 800 K from low temperature phase (Pnma) to high temperature phase (Cmcm) [10]. The band structure is anisotropic due to the layered structures and this is reflected in the anisotropic transport properties. The highest thermoelectric performance is obtained along the b-c plane in SnSe, and the distorted SnSe<sub>7</sub> polyhedra exhibit anharmonic bonding and zig-zag Sn-Se structures along the b- or c-axis resulting in the very low thermal conductivity without

nanostructuring .

Although several theoretical studies on the electronic structure of SnSe have been performed and are consistent with the transport properties [11-14], a spectroscopic study on the electronic structure may provide useful information to understand the physical properties. In particular, it is rather difficult to estimate the effect of Na doping from the theoretical calculation since it is expected to introduce atomic and electronic disorder to the system in a complicated manner. In this context, it is highly important to study the electronic structure of SnSe and Na-doped SnSe using spectroscopic methods. In the present work, we report an angle-resolved photoemission spectroscopy (ARPES) study on SnSe and  $\text{Sn}_{0.985}\text{Na}_{0.015}\text{Se}$  single crystals.

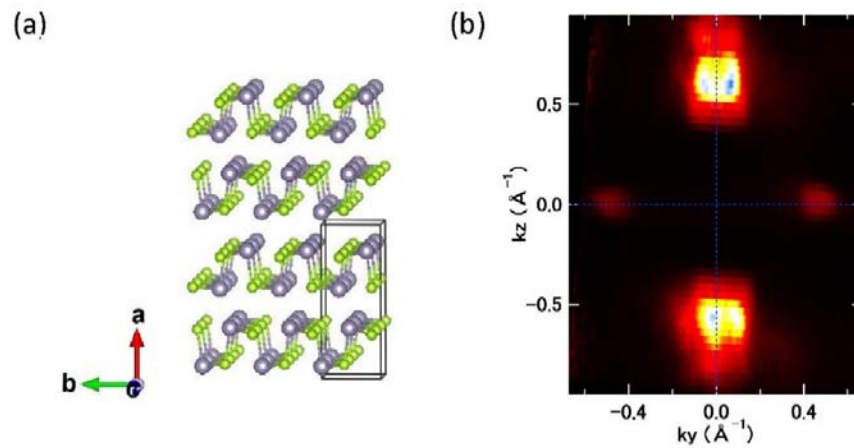


FIG. 1: (Color online) (a) Crystal structure of SnSe created by VESTA [10].

(b) Photoemission intensity map in the  $k_y$ - $k_z$  plane at 0.195 eV for Na-doped SnSe.  $k_y$  and  $k_z$  are wave numbers along the  $\Gamma$ -Y and  $\Gamma$ -Z directions corresponding to the b-axis and c-axis directions, respectively.

Single crystals of SnSe and  $\text{Sn}_{0.985}\text{Na}_{0.015}\text{Se}$  (substitutional Na dopants) were grown as reported in the literature [1]. ARPES measurements were performed at beamline 9A of Hiroshima Synchrotron Radiation Center(HiSOR). The base pressure of the spectrometer of HiSOR BL-9A was in the  $10^{-9}$  Pa range. The crystals were cleaved at 300 K under the ultrahigh vacuum and then cooled to 20 K for the ARPES measurements. The ARPES data were obtained within 12 hours after the cleavage. The excitation energy was set to 22.8 eV corresponding to  $k_x \sim 8\pi/a$  (wave number perpendicular to the surface) in order to observe the valence band top near the Z point. Binding energies were calibrated using the Fermi edge of gold reference samples. The total energy resolution was 22 meV.

Figure 1(b) shows the photoemission intensity map in the  $k_y$ - $k_z$  plane at binding energy of 0.195 eV for Na-doped SnSe ( $\text{Sn}_{0.985}\text{Na}_{0.015}\text{Se}$ ). Here,  $k_y$  and  $k_z$  are wave numbers along the  $\Gamma$ -Y and  $\Gamma$ -Z directions, respectively. The valence-band maxima near the Z point are clearly

observed. The band dispersions of the  $\Gamma$ -Z ( $k_z$ ) cut near the valence-band maxima are shown in Fig. 2 for SnSe and Na-doped SnSe. In SnSe, the two valence-band maxima are observed. This observation is consistent with the recent ARPES works by Wang *et al.* [15] and Pletikosić *et al.* [16] In our samples, the energy position of the valence band maxima is  $\sim 200$  meV below the Fermi level ( $E_F$ ) as shown in Fig. 2(a) whereas they are touching  $E_F$  in the work by Wang *et al.* [15] This indicates that the SnSe crystals studied by Wang *et al.* are hole doped due to some defects. On the other hand, the present SnSe crystals have less defects which is important for achieving higher mobility. In the study by Pletikosić *et al.* [16], the energy position of the valence band maxima is  $\sim 120$  meV below  $E_F$  which is slightly smaller than the present result. The overall agreement with the observed band dispersion and the band structure calculation is reasonably good. In the Na-doped SnSe, the entire valence band is shifted upwards by  $\sim 200$  meV and the valence band maxima touch  $E_F$ , indicating that Na-doped SnSe is a degenerate semiconductor.

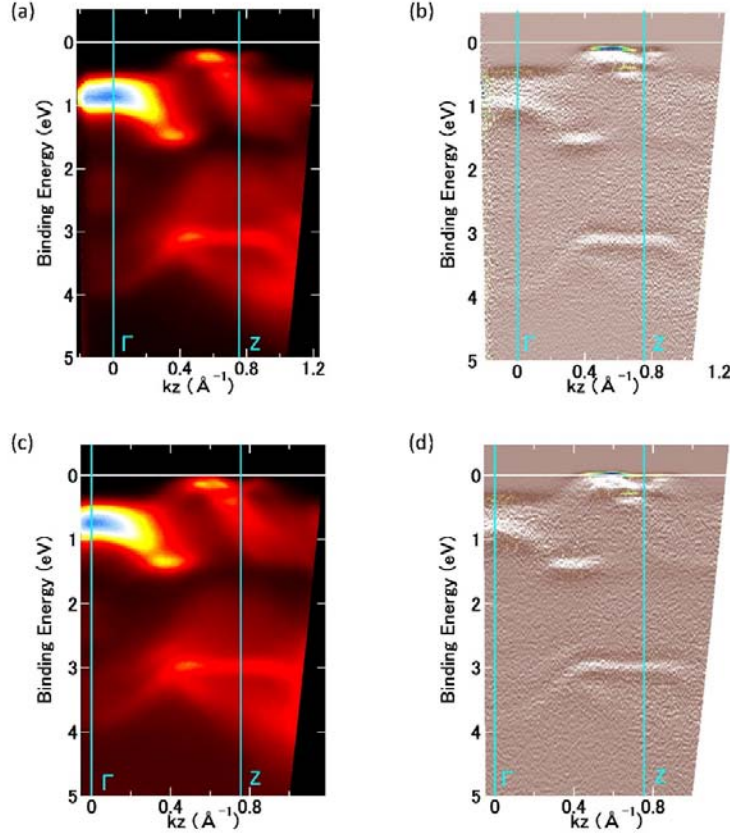


FIG. 2: (Color online) (a) Photoemission intensity map along the  $\Gamma$ -Z direction ( $k_z$  cut) for undoped SnSe. (b) Second derivative (with respect to energy) map along the  $k_z$  cut for undoped SnSe. (c) Photoemission intensity map along the  $k_z$  cut for Na-doped SnSe. (d) Second derivative (with respect to energy) map along the  $k_z$  cut for Na-doped SnSe.

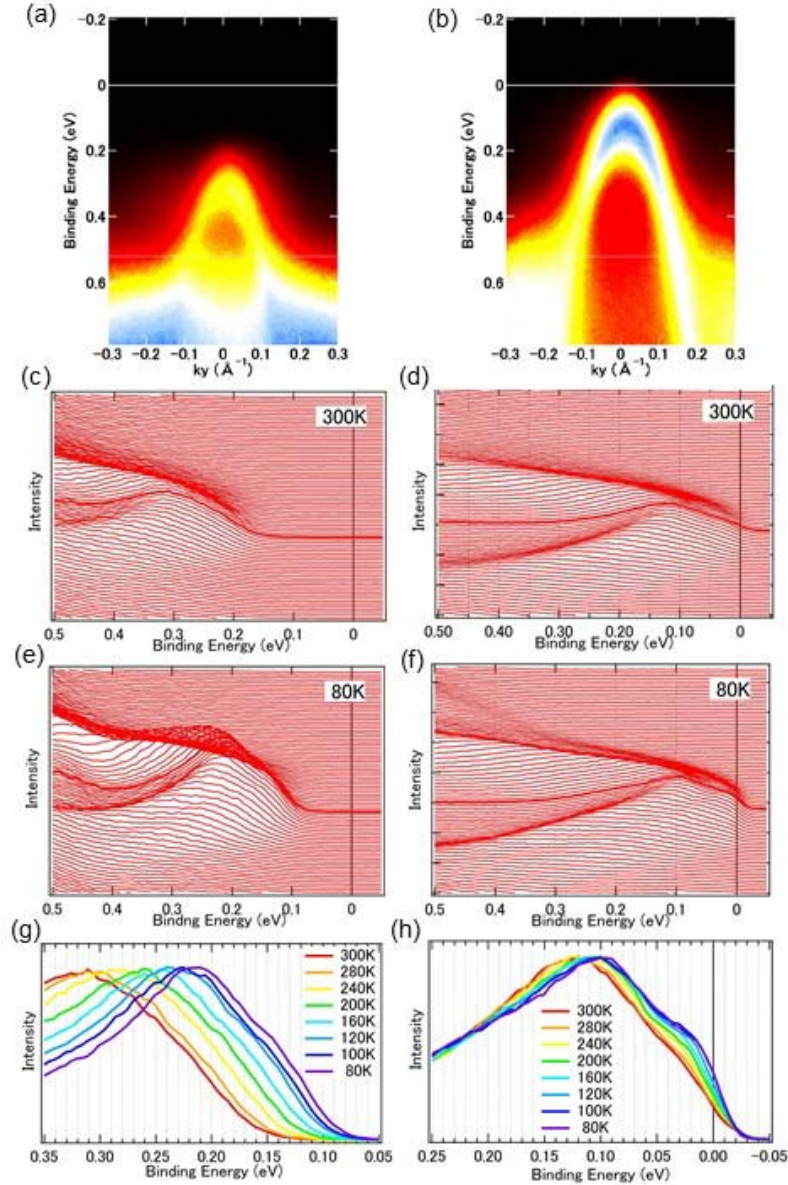


FIG. 3: (Color online) Photoemission intensity map of the  $k_y$  cut at 300 K crossing the band maximum (a) for SnSe and (b) for Na-doped SnSe. Energy distribution curves at 300 K including the band maximum (c) for SnSe and (d) for Na-doped SnSe. Energy distribution curves at 80 K including the band maximum (e) for SnSe and (f) for Na-doped SnSe. Temperature evolution of the energy distribution curve at the band maximum (g) for SnSe and (h) for Na-doped SnSe.

Figures 3(a) and (b) show band dispersions of the  $\Gamma$ -Y ( $k_y$ ) cut at 300 K crossing the band maximum for SnSe and Na-doped SnSe, respectively. The chemical potential shift of  $\sim 200$  meV by the Na-doping is clearly seen. The present results support the canonical hole dope picture of the Na doping. In Figs. 3(c) and (d), energy distribution curves including the band

maximum at 300 K are plotted for SnSe and Na-doped SnSe in order to show the effect of the Na-doping on the spectral shape. At 300 K, the valance band is shifted towards  $E_F$  without appreciable spectral change. In Figs. 3(e) and (f), energy distribution curves at 80 K are also plotted for SnSe and Na-doped SnSe. In going from 300 K to 80 K, the valance band is shifted towards  $E_F$  with appreciable spectral change both in SnSe and Na-doped SnSe. In order to show the temperature evolution, the energy distribution curves at the band maximum are compared in Figs. 3(g) and (h) for SnSe and Na-doped SnSe, respectively.

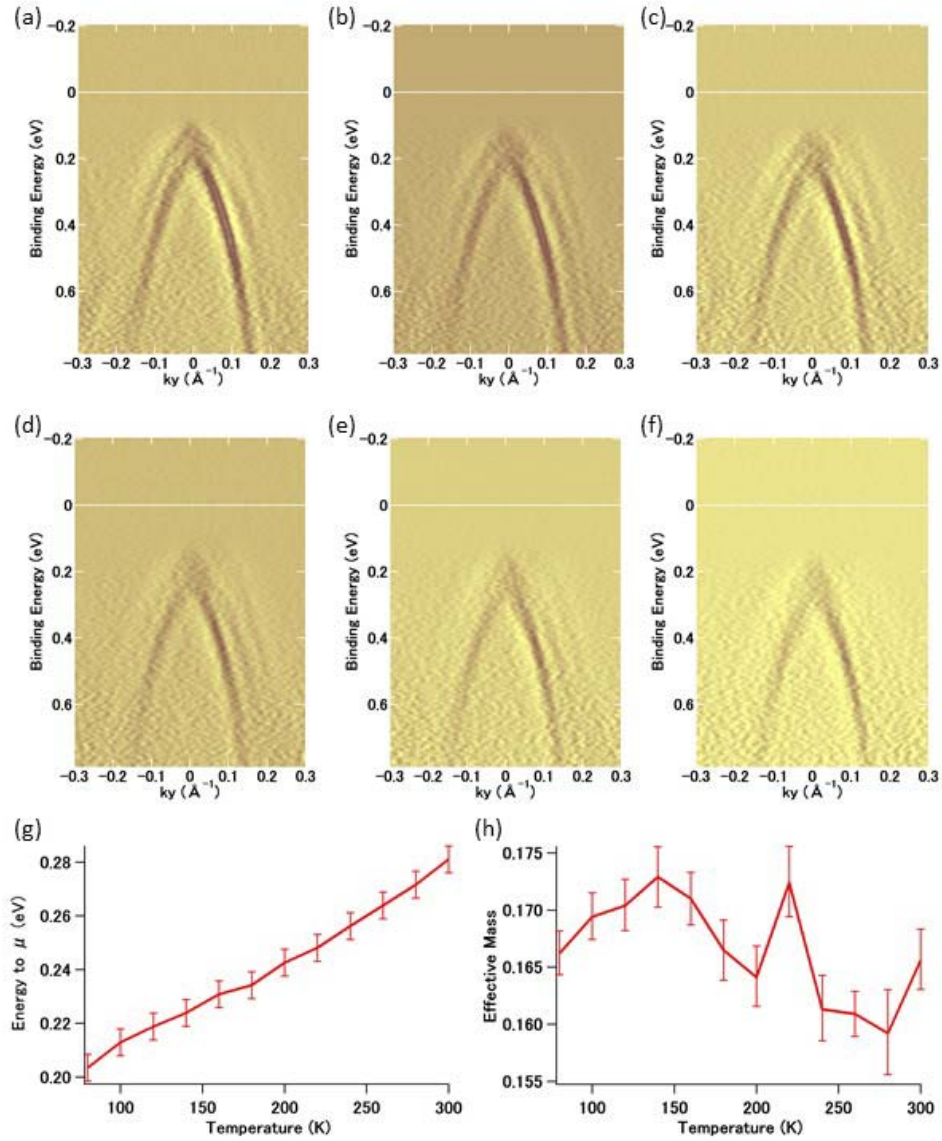


FIG. 4: (Color online) Temperature evolution of the second derivative (with respect to  $k_y$ ) map along the  $k_y$  cut for SnSe at (a)80, (b)120, (c)160, (d)200, (e)240, (f)280K. (g) Energy difference between the valence band top (peak position) and the chemical potential  $\mu$ . (h) Effective mass along the  $k_y$  direction as a function of temperature.

Figures 4(a)-(f) show temperature evolution of the band dispersion along the  $k_y$  cut for SnSe. In going from 80 K to 280 K, the valence band maximum is shifted away from  $E_F$  by the depletion of the thermally excited holes in the valence band. **Although the spectral shape changes with temperature, the peak position can be roughly estimated by fitting the energy distribution curves to Gaussian functions with Shirley background.** Figure 4(g) shows temperature dependence of the energy difference between the valence band top (peak position) and the chemical potential  $\mu$  for SnSe, indicating that the chemical potential shift is  $\sim 80$  meV between 80 K and 280 K at SnSe. In a semiconductor, the slope of this plot corresponds to Seebeck coefficient. Indeed, the slope of  $\sim 0.4$  meV/K is comparable to the reported value for SnSe at room temperature. The band dispersion is obtained from second derivative with respect to  $k_y$ . The effective mass along the  $k_y$  cut is estimated to be  $\sim 0.17m_e$  as shown in Fig. 4(h) in agreement with Pletikosić *et al.* [16]

Figures 5(a)-(f) show temperature evolution of the band dispersion of the  $k_y$  cut for Na-doped SnSe. Figure 5(g) shows temperature dependence of the energy difference between the valence band top (peak position) and  $\mu$ . This result indicates that the chemical potential shift is  $\sim 30$  meV between 80 K and 280 K which is much smaller than SnSe. In a degenerate semiconductor or a metal, the slope of this plot does not correspond to Seebeck coefficient. However, this value  $\sim 0.15$  meV/K is consistent with the Seebeck coefficient of Na-doped SnSe at room temperature suggesting that thermal excitation of holes from the localized acceptor level governs the chemical potential shift. This is probably related to the fact that, although the valence band maxima or the low energy tail of the photoemission peak touches  $E_F$ , the peak position is still around  $\sim 70$  meV below  $E_F$  at 80 K. In addition, the effective mass along  $k_y$  exhibits anomalous temperature dependence as shown in Fig. 5(h). The effective mass takes its maximum at  $\sim 200$  K indicating that band renormalization due to electron-lattice interaction plays important roles. It is tempting to speculate that the anomalous temperature evolution of chemical potential and effective mass is associated with underlying lattice instability in Na-doped SnSe. The peak position is employed to estimate the chemical potential shift and the effective mass. In addition to the dispersion of the peak position, the low energy tail is seen in the second derivative maps for SnSe and Na-doped SnSe in Figs. 4 and 5. The low energy tail reaches  $E_F$  by the hole doping. The present ARPES results suggest that the Na-doped SnSe harbors a novel metallic state associated with the multi-band nature of Sn 5p and the strong electron-lattice coupling.

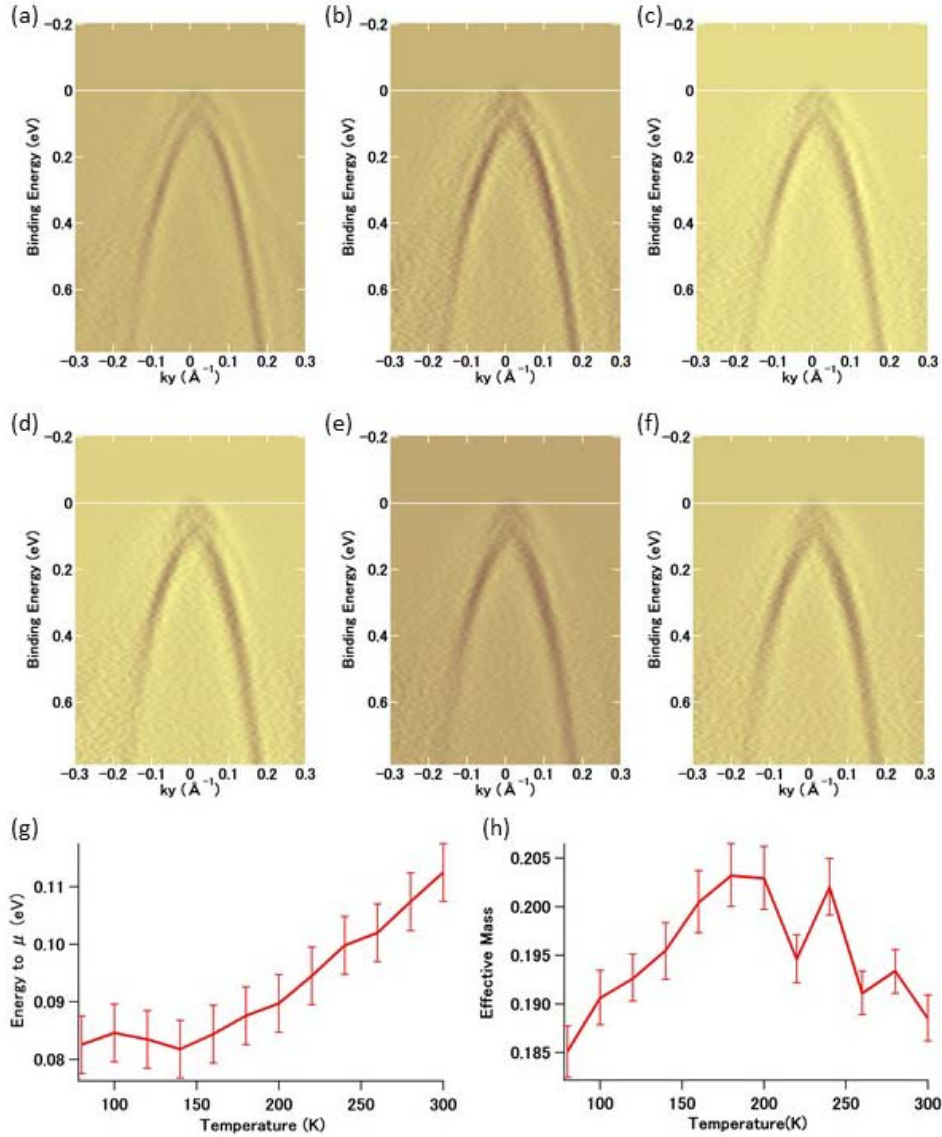


FIG. 5: (Color online) Temperature evolution of the second derivative (with respect to  $k_y$ ) map along the  $k_y$  cut for Na-doped SnSe at (a)80, (b)120, (c)160, (d)200, (e)240, (f)280K. (g) Energy difference between the valence band top (peak position) and the chemical potential  $\mu$ . (h) Effective mass along the  $k_y$  direction as a function of temperature.

In conclusion, we have studied the electronic structure of SnSe and Na-doped SnSe by means of ARPES. The valence band top reaches  $E_F$  by the Na doping, and Na-doped SnSe can be viewed as a degenerate semiconductor which is consistent with the transport properties. However, the chemical potential shift with temperature is unexpectedly large, apparently inconsistent with the degenerate semiconductor picture. The conflicting observations suggest that the holes in Na-doped SnSe cannot be described by a simple itinerant picture or by a simple impurity level picture. In addition, whereas the low energy

tail of the photoemission peak touches  $E_F$ , the peak position is still below  $E_F$  in Na-doped SnSe. This behavior indicates strong electron-lattice coupling probably due to multi-band nature of Sn 5p. These results suggest that, in order to better understand the novel metallic state of Na-doped SnSe, the low temperature transport properties of single crystals and their doped versions must be investigated in detail.

The authors would like to thank Y. Chiba and S. Suzuki for their contributions in the early stage of this work. This work was supported by CREST-JST (Grant No. JPMJCR15Q2). The synchrotron radiation experiment was performed with the approval of HiSOR (2015-A-5).

## References

- <sup>1</sup> L.-D. Zhao, G. Tan, S. Hao, J. He, Y. Pei, H. Chi, H. Wang, S. Gong, H. Xu, V. P. Dravid, C. Uher, G. J. Snyder, C. Wolverton, and M. G. Kanatzidis, *Science* **351**, 141 (2016).
- <sup>2</sup> C. W. Li, J. Hong, A. F. May, D. Bansal, S. Chi, T. Hong, G. Ehlers, and O. Delaire, *Nat. Phys.* **11**, 1063 (2015).
- <sup>3</sup> J. P. Heremans, V. Jovovic, E. S. Toberer, A. Saramat, K. Kurosaki, A. Charoenphakdee, S. Yamanaka, and G. J. Snyder, *Science* **321**, 554 (2008).
- <sup>4</sup> Y. Pei, X. Shi, A. LaLonde, H. Wang, L. Chen, and G. J. Snyder, *Nature* **473**, 66 (2011).
- <sup>5</sup> Y. Pei, H. Wang, and G. J. Snyder, *Adv. Mater.* **24**, 6125 (2012).
- <sup>6</sup> K. Biswas, J. He, I. D. Blum, C. I. Wu, T. P. Hogan, D. N. Seidman, V. P. Dravid, and M. G. Kanatzidis, *Nature* **489**, 414 (2012).
- <sup>7</sup> H. J. Wu, L. D. Zhao, F. S. Zheng, D. Wu, Y. L. Pei, X. Tong, M. G. Kanatzidis, and J. Q. He, *Nat. Commun.* **5**, 4515 (2014).
- <sup>8</sup> L.-D. Zhao, S.-H. Lo, Y. Zhang, H. Sun, G. Tan, C. Uher, C. Wolverton, V. P. Dravid, and M. G. Kanatzidis, *Nature* **508**, 373 (2014).
- <sup>9</sup> G. Tan, L.-D. Zhao, F. Shi, J. W. Doak, S.-H. Lo, H. Sun, C. Wolverton, V. P. Dravid, C. Uher, and M. G. Kanatzidis, *J. Am. Chem. Soc.* **136**, 7006 (2014).
- <sup>10</sup> T. Chattopadhyay, J. Pannetier, and H. G. Von Sshnering, *J. Phys. Chem. Solids* **47**, 879 (1986).
- <sup>11</sup> R. Car, G. Ciucci, and L. Quartapelle, *Phys. Stat. Sol.* **86**, 471 (1978).
- <sup>12</sup> L. Makinistian and E. A. Albanesi, *Phys. Status Solidi B* **246**, 183 (2009).
- <sup>13</sup> K. Kutorasinski, B. Wiendlocha, S. Kaprzyk, and J. Tobola, *Phys. Rev. B* **91**, 205201 (2015).
- <sup>14</sup> G. Shi and E. Kioupakis, *J. App. Phys.* **117**, 065103 (2015).
- <sup>15</sup> Z. Wang, C. Fan, Z. Shen, C. Hua, Q. Hu, F. Sheng, Y. Lu, H. Fang, Z. Qin, J. Lu, Z.-A. Xu, D. W. Shen, and Y. Zheng, *Nature Commun.* **9**, 47 (2018).
- <sup>16</sup> I. Pletikosić, F. von Rohr, P. Pervan, P. K. Das, I. Vobornik, R. J. Cava, and T. Valla, arXiv:1707.04289v1.